The first original version of this manuscript has been submitted on October 14th, 2022, for consideration in the peer-reviewed Solar Energy journal. Please note that the manuscript has not undergone peer review yet and has not been formally accepted for publication. Subsequent versions of this manuscript may have slightly different content. Please feel free to contact any of the authors; we welcome feedback.

Solar irradiance distribution under vertically mounted agrivoltaic systems – Model development, validation, and applications for microclimate assessment

Pietro Elia Campana[1,*], Jonathan Staaf Scragg[2], Silvia Ma Lu[1], Sebastian Zainali[1], Bengt Stridh[1], Stefano Amaducci[3], Michele Colauzzi[3]

[1] Mälardalen University, Future Energy Center, BOX883, Västerås, Sweden

[2] Uppsala University, Solar Cell Technology Division, Department of Materials Science and Engineering, Regmentsvägen 1 Uppsala, Sweden

[3] Università Cattolica del Sacro Cuore, Department of Sustainable Crop Production, Via Emilia Parmense 84, Piacenza, Italy

Abstract

Accurate assessment of the Photosynthetically Active Radiation (PAR) and Global Horizontal Irradiance (GHI) at the crop level is paramount for accurately assessing the energy balances and the crop yield under agrivoltaic systems. The shadings produced by the photovoltaic modules and structures of the agrivoltaic systems cause a non-homogeneous distribution of PAR and GHI at the crop level. It is thus essential to calculate their distribution at a high spatial resolution within the agrivoltaic field. Using field data and commercial software, we have validated a high spatial resolution model (i.e., 25 cm × 25 cm) for PAR and GHI distribution within a vertical agrivoltaic system. The results show good model accuracy with coefficients of determination higher than 0.98 when comparing GHI from the model developed in this study and commercial software based on ray tracing. Model applications are presented with consideration to the computation of surface temperature, evapotranspiration, crop yield, and soil moisture. The model developed in this study shows good agreement in terms of crop yield computations as compared to a previously published model for agrivoltaic systems simulations and optimization (Campana et al., 2021). The added value of the model presented in this study consists in performing high spatial resolution computations of microclimatic parameters and crop yield within the agrivoltaic field.

* Corresponding author: pietro.campana@mdu.se

1 Introduction

In 2021, worldwide, 167.8 GW_p of solar photovoltaic (PV) capacity was installed, about 56% of the total newly installed renewable energy capacity (SolarPower Europe, 2022). Despite the COVID-19 pandemic challenges, utility-scale PV systems remained the largest segment, with 90.7 GW_p installed and a levelized cost of electricity lower than any other type of conventional energy conversion system (SolarPower Europe, 2022). Typically, PV is installed on flat land with good insolation. Frequently this land is, or could potentially become, agricultural land, because the exact requirements apply for both lands uses. The permitting process for installing PV plants on (actual or potential) agricultural land is a significant challenge due to the so-called "food-versus-fuel (electricity)" debate (Tomei and Helliwell, 2016; Ketzer et al., 2020; Campana and Lawford, 2022). This ethical debate concerns whether the land must be used for energy conversion or food production.

Agrivoltaic systems are one of the solutions to avoid such competition and simultaneously attain conflicting Sustainable Development Goals (SDGs), i.e., Goal 2 (Zero hunger), and Goal 7 (Affordable and clean energy). Agrivoltaic systems allow the coexistence of agricultural activities and electricity production through the exploitations of unique supporting structures for the PV systems, i.e., stilt-mounted systems with fixed and tracking PV array, vertically mounted PV systems with bifacial PV modules, or overhead structures (Horowitz et al., 2020). Those structures allow conventional agricultural machinery to perform traditional agricultural practices underneath or between the PV arrays.

The combination of PV electricity production and conventional agriculture presents several synergies. From the PV perspective, this combination allows higher solar energy conversion efficiencies because the microclimate produced by the crops can lead to a lower solar cell operating temperature (Barron-Gafford et al., 2019). Moreover, the configuration of the PV modules' supporting structure and the higher elevation of the PV modules compared to conventional ground-mounted PV systems leads to higher convectional cooling (i.e., higher windspeed or airflow) and, thus, again, lower solar cell operating temperatures (Johansson et al., 2022). Combining crops and bifacial PV modules can increase the specific electricity production per m2 when the crops are specifically selected to increase albedo during the crop growing season. The enhanced reflected irradiance increases PV production from both the front and rear sides of the PV modules (Marion, 2022; Riedel-Lyngskær et al., 2022; Sieber et al., 2022). From the crop production perspective, the presence of PV modules and the shading

produced by the PV modules can – within limits – reduce water and temperature stresses by altering the energy balance at the crop level (Amaducci et al., 2018). The PV modules and the supporting structure can beneficially alter the crop's wind speed distribution, avoiding soil erosion and evapotranspiration (Zainali et al., 2022). Agrivoltaic systems with overhead structures can also protect crops from extreme weather events and, at the same time, provide an opportunity for water harvesting (Al Mamun et al., 2022). Potential disadvantages of agrivoltaic systems include uneven precipitation distribution that can lead to increased runoff, erosion, and soil compaction Elamri et al. (2018). The PV modules supporting structures reduce the effective usable agricultural areas. Trommsdorff et al. (2021) reported an 8.3% loss of the total cultivated area for an overhead agrivoltaic system. Campana et al. (2021) reported a land loss of 0.5 m left and right of the supporting structure axis for vertically mounted agrivoltaic systems, which corresponds to a 10% loss of productive land in vertically mounted agrivoltaic system with a 10 m row distance. This land loss translates to reduced yield per hectare and income from crop production for the farmers. The reduced and heterogenous cumulative solar irradiation at the crop level can negatively affect crop yield and crop yield distribution. Other disadvantages include damage of agricultural machinery to the PV modules and PV modules supporting structure.

The accurate assessment of the Photosynthetically Active Radiation (PAR) and the Global Horizontal Irradiance (GHI) at the crop level is of paramount importance for accurately assessing the crop yield under agrivoltaic systems and the energy balances at the crop level. The shadings produced by the PV modules and structures of the agrivoltaic systems cause a non-homogeneous distribution, spatially and temporally, of PAR and GHI at the crop level. It is thus essential to calculate these distributions at a high spatial and temporal resolution within the agrivoltaic field. The crop yield is proportional to PAR (Williams et al., 1989), which, in the case of agrivoltaic systems, is reduced compared to open-field conditions due to the shadings produced by the PV modules and supporting structures at the crop level. The crop yield under agrivoltaic systems does not depend only on PAR. It depends on the leaf area index (LAI) that for certain crops increases under shading conditions for compensating the reduced light (Marrou et al., 2013), and it also depends on the crop growth-regulating stress factors, such as the water stress connected to the evapotranspiration process and the temperature stress of the crop. The shading of the PV modules and the supporting structures reduces PAR and GHI, which is of fundamental importance in the energy balances for calculating evapotranspiration, ground temperature, and, generally, the microclimate under agrivoltaic

systems. This study will primarily focus on PAR and GHI assessment and their effects on evapotranspiration, surface temperature, soil moisture, and crop yield. Although there have been several studies attempting to calculate and visualize PAR and GHI distributions at the crop level (Amaducci et al., 2018: Campana et al., 2021; Katsikogiannis et al., 2022), few works have focussed on validating the actual time series of PAR and GHI behind the spatially distributed grid cells. Moreover, little work has been done on the mathematical modelling of the microclimate under agrivoltaic systems resulting from the variation of GHI distribution due to shadings. Significantly few studies on microclimate modelling under agrivoltaic systems exist (Zainali et al., 2022).

Recently, ray tracing approaches, which depict how light rays propagate through space and interact among objects considering reflection and absorption processes, have been developed and implemented to assess the performance of bifacial PV modules more accurately, especially for the assessment of the backside irradiance (Lo et al., 2015; Deline et al., 2016; Katsikogiannis et al., 2022). Several research studies have compared the backside irradiance assessment using ray tracing vs view-factor approaches. The view factor approach assumes that the reflected radiation is isotropic and is calculated through integration methods (Hansen et al., 2017; Sun et al., 2018). Pelaez et al. (2018) compared different software packages using different approaches (view factor, ray tracing, and empirical models [i.e., relationships based on measured back surface irradiance]) to calculate back surface irradiance in PV systems with bifacial modules. The authors concluded that there was a good agreement between simulations performed by the investigated software and the measurements, especially at low ground clearance conditions. The National Renewable Energy Laboratory (NREL) view factor model agreed well with Radiance (Ward, 1994). At higher ground clearance values, the influence of edge effects becomes more pronounced, and few methods/models could depict these effects. The view factor and radiance-based models agreed well with the measurements overall in the examined studies. A detailed model based on the view factor approach to depict the back surface irradiance on the edges was developed by Hansen et al. (2016) and compared with a radiance-based model. A similar comparison was carried out by Riedel-Lyngskær et al. (2020) using eighth software, among commercially available, freeware, and open-source software for bifacial PV systems modelling. Seven of the investigated software use a 2D view factor approach, while one uses a 3D ray tracing approach. The view factor approach produced results within ±1% of the measured monthly bifacial gain for the fixed-tilt system. Nevertheless, less accuracy was attained for the single-axis tracker systems. Despite the research activities conducted so far on

the use of view factor and ray tracing methods for back surface irradiance, little work has been done on raytracing methods to calculate solar irradiance at the ground level under agrivoltaic systems and on the comparison between view factor and raytracing methods.

In-depth research in this field is motivated by the lack of knowledge on how shading affects solar radiation distribution and energy balances at ground level and how the induced microclimate (i.e., ground temperature, evapotranspiration, PAR, and GHI) affects both crop and energy conversion. Differently from conventional open-field conditions, crops under agrivoltaic systems do not receive PAR total but a combination of PAR total and PAR diffuse that can affect crop radiation use efficiency. Crop growth under PAR diffuse conditions is more efficient than PAR beam conditions (Cheng et al., 2015). Assessing solar irradiance distribution at the ground level is paramount for the simultaneous and synergistic co-optimization of PV and agricultural yields that typically have conflicting objectives. For instance, conventional PV yield optimization might lead to a PV system design that reduces ground irradiance to unacceptable levels to maintain high crop yields. On the other hand, crop yield optimization might lead to PV system designs that are far from optimal from a cost-benefit perspective. This study's contribution is to extend the model developed by Campana et al. (2021) to accurately depict PAR and GHI distribution at the ground level, providing validation and cross-validation. Moreover, some critical applications of the model to depict microclimatic conditions under agrivoltaic systems are also presented.

The remainder of the paper is organized as follows: Section 2 describes the model development, the experimental site used for validation, and the further development of the model to depict microclimatic conditions under agrivoltaic systems; Section 3 presents the main results of the study in terms of validation with measurements data and cross-validation with a 3D raytracing commercial software. At the same time, microclimatic conditions under the investigated and modelled agrivoltaic systems are presented and discussed. Section 4 concludes the study.

2 Methods and data

2.1 Model development

The model presented in this study is an enhanced version of the model by Campana et al. (2021), especially for what concerns the solar radiation model for the high spatial distribution of PAR and GHI. In Campana et al. (2021), the shading matrix required for calculating both the beam and diffuse shading factors was calculated for one single point, corresponding to the centre of

the area comprised between two rows of the vertically mounted agrivoltaic system, as shown in Figure 1 (left). The model geometry refers to the first agrivoltaic system installed in Sweden installed at Kärrbo Prästgård (59.55°N, 16.75°E) and is composed of three vertical rows of approximately 18 m in length with 10 m row spacing. In the new model, the area within two neighbouring rows of the agrivoltaic system is discretized with a mesh of 25 cm × 25 cm, and the shading matrix is calculated for each grid cell (Figure 1 [right]). The model by Campana et al. (2021) has been optimized to reduce computational time. All the results presented in this study refer to a sky dome discretization of 1°. This is particularly important for calculating the diffuse shading factors since each grid cell has its own characteristic sky dome area that is obstructed by the vertically mounted bifacial PV modules. See, for instance, Figure 2, where two photos are taken with a fisheye lens at two different points within the agrivoltaic row. The figure clarifies the importance of the view factor and, at the same time, shows that a single point in the centre (see Figure 1) could represent an oversimplification of reality.

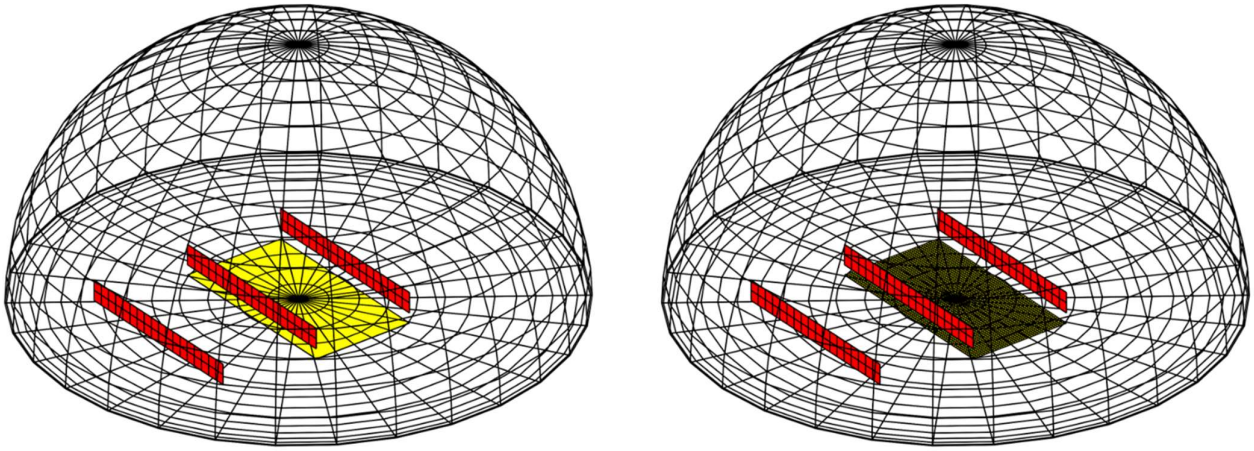

Figure 1: Agrivoltaic system layout and sky-dome discretization (here at 10° only for illustration purposes). The yellow area is the reference area assumed as a single rectangle by Campana et al. (2021) (left) while discretized at 25 cm × 25 cm in this study (right).

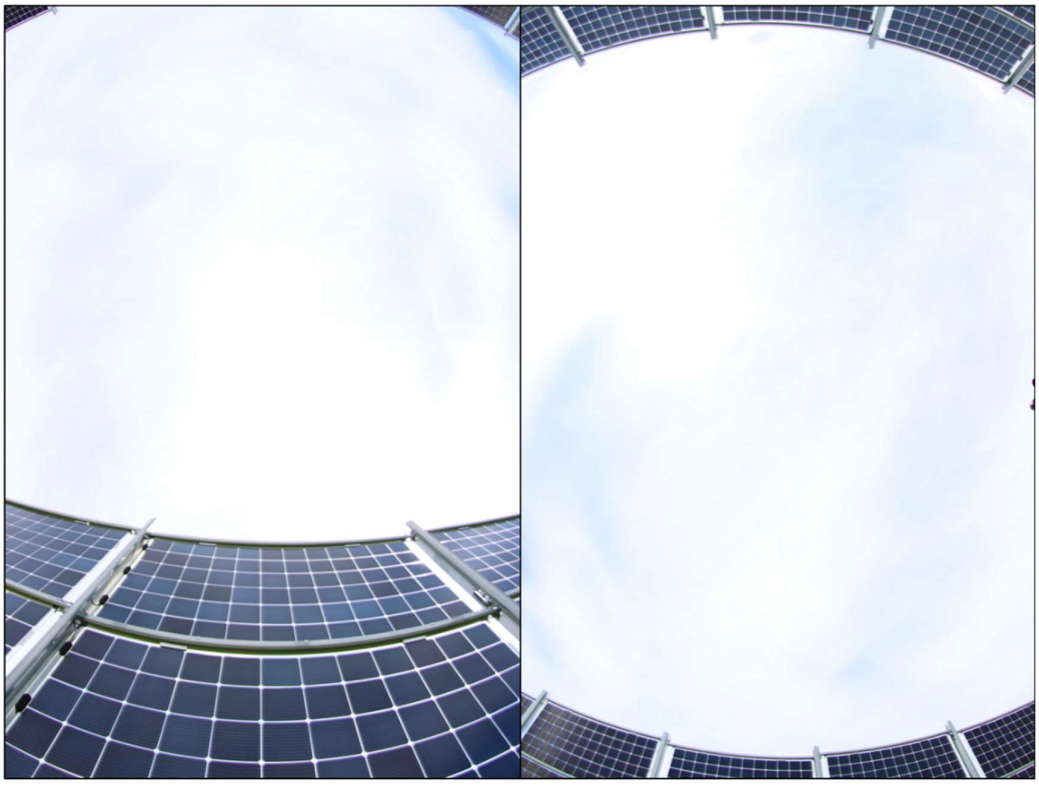

Figure 2: Part of the sky visible by two different points (i.e., at 50 cm from the east row [left], and in the middle of the row [right]) within one agrivoltaic row. Photos taken the 14th of July 2022 with a fisheye lens.

For each simulation time step and grid cell composing the reference area, the algorithm assigns a Boolean variable to check if the beam irradiance reaches the cell or not. This computation is performed by combining the information concerning the solar position with the information concerning the shadings. The solar radiation position model is from Koblick (2009), while the shading model uses the approach developed by Cascone et al. (2011). For computational time constraints, the diffuse shading factor is calculated according to the simplified method by Quaschning and Hanitsch (1995), compared to Campana et al. (2021), where a radiance-based approach was implemented. If the specific grid cell does not receive any beam irradiance for a single time step between sunrise and sunset, the resulting total radiation is given by the diffuse irradiance multiplied by the diffuse shading factor. Contrarily, if the grid cell receives the beam irradiance, the total irradiance is given by the sum of the beam irradiance and the diffuse irradiance multiplied by the diffuse shading factor. The diffuse component of the PAR is calculated with the Starke model, initially developed by Starke et al. (2018) for GHI decomposition and cloud enhancement detection and implemented for PAR decomposition and

reparametrized for Sweden by Ma Lu et al. (2022). The following equation gives the original Starke model:

$$k_d^{Starke} = \begin{cases} \dfrac{1}{1 + e^{\beta_7+\beta_8 k_t+\beta_9 AST+\beta_{10}\theta_z+\beta_{11}K_T+\beta_{12}\psi+\frac{\beta_{13}G_{cs}}{277.78}}}, & k_{CSI} \geq 1.05 \text{ and } k_t > 0.65 \\ \dfrac{1}{1 + e^{\beta_0+\beta_1 k_t+\beta_2 AST+\beta_3\theta_z+\beta_4 K_T+\beta_5\psi+\frac{\beta_6 G_{cs}}{277.78}}}, & \text{otherwise} \end{cases}, \quad (1)$$

where, k_d^{Starke} is the diffuse fraction, k_t is the clearness index, AST is the apparent solar time (h), θ_z is the zenith angle (°), K_t is the daily clearness index, ψ is three-point moving average of clearness index, G_{cs} is the clear sky irradiance (W/m^2), and k_{CSI} is the clear-sky index. The coefficients β_0-β_{13} for PAR decomposition can be found in the study by Ma Lu et al. (2022). Since the original Starke model was for decomposing GHI and not for PAR, the relationship developed by Spitters et al. (1986) is employed to calculate the actual PAR diffuse fraction k_{d_PAR}:

$$k_{d\_PAR} = \frac{\left[1 + 0.3\left(1 - (k_d^{Starke})^2\right)\right] k_d^{Starke}}{1 + \left(1 - (k_d^{Starke})^2\right)\cos^2(90 - \alpha)\cos^3\alpha}, \quad (2)$$

where, α is the solar elevation angle (º). The PAR reflection component has been calculated with a view factor approach. The view factor has been calculated with a Monte Carlo Analysis as described in the study by Martinez (2013) and refers to the case of a "Rectangular plate to unequal rectangular plate" (Howell, 1992; Siegel and Howell, 2002). It is mathematically defined in Equation 3 and depicted in Figure 3.

$$F_{1\to2} = \frac{A_2}{n}\sum_{i=1}^{n}\frac{\cos\beta_1\cos\beta_2}{\pi r_{12}^2}\bigg|_i = \frac{WL}{n}\sum_{i=1}^{n}\frac{zx}{\pi[(x^2 + z^2 + (y_2 - y_1)^2)]^2}\bigg|_i, \quad (3)$$

where, $F_{1\to2}$ is the view factor estimating the PAR reflected by the vertical surface that impinges on the horizontal surface, n is the number of randomly selected pair of coordinates (i.e., 1000 in our study), β_1 and β_2 are the angles defining the orientation of the two infinitesimal surfaces dA_1 and dA_2 respective to the line of the centres (°), r_{12} is the distance between the two infinitesimal surfaces (m), and W, L, x, y, z are distances/coordinates defined in Figure 3. The total PAR hitting on the vertical surface has been calculated from the total, beam, and diffuse PAR on the horizontal surface by applying the Perez 1990 transposition model (Perez et al., 1987; Perez et al., 1990) available in the PV_LIB (Sandia National Laboratories, 2022).

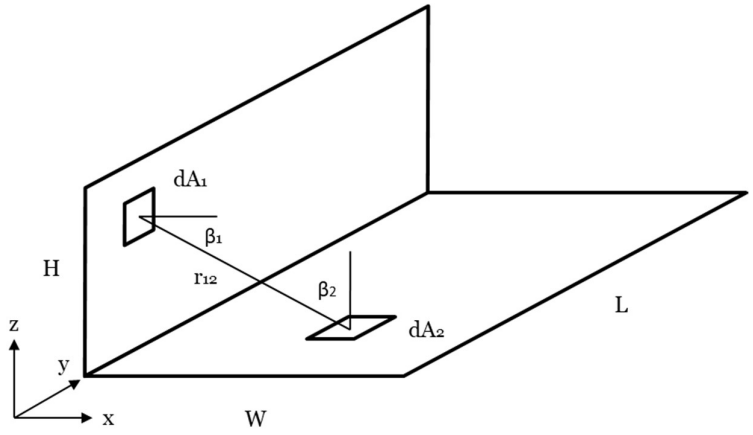

Figure 3: View factor approach.

The reflected PAR at ground level has been computed as the product of the global tilted PAR, view factor, and albedo of the PV modules. The albedo of the PV modules has been assumed equal to 4.7% as retrieved from DL-Light® material properties database (Spectral Materials Database, 2022; Alstan Jakubiec, 2016; Alstan Jakubiec, 2022). Interreflections were not computed.

2.2 Applications

Three potential applications of the model developed in Section 2.1 are further investigated in this study to show the PAR/GHI distribution effects and model potentials. These include surface temperature, evapotranspiration, soil moisture, and crop yield distribution under agrivoltaic systems. The surface temperature T_s (°C) has been estimated with the methods by Remund et al. (2018) with the following relationship for the daytime:

$$T_s = T_a + [0.015 * (1 - \rho) * GHI - 0.7] * e^{-0.09*v}, \quad (4)$$

where, T_a is the ambient temperature (°C), ρ is the albedo, and v is the wind speed (m/s). It must be pointed out that agrivoltaic systems, particularly vertically mounted agrivoltaic systems, can significantly affect wind speed and direction. The rows of PV panels create a wind barrier in one direction, while they can channel the wind in the opposite direction (i.e., vertically mounted agrivoltaic systems with PV rows aligned in the North-South direction can significantly affect the wind with East-West direction while increasing winds coming from the North-South direction) (Kuoet al., 2020). This effect has not been considered in the application of Equation 4. The hourly reference evapotranspiration (ET_o) (mm/h) has been computed with the Penman-Monteith equation (Allen et al., 1998; Zotarelli et al. (2010) as follows:

$$ET_o = \frac{0.408\Delta(R_n - G) + \gamma \frac{37}{T_a + 273} u_2 (e_s - e_a)}{\Delta + \gamma(1 + 0.34v)}, \quad (5)$$

where, Δ is the saturation slope of the vapor pressure curve at T_a (kPa/°C), R_n is the net hourly radiation (MJ/m^2/hour), G is the hourly soil heat flux density (MJ/m^2/hour), γ is the psychrometric constant (kPa/°C), T is the hourly air temperature (°C), e_s is saturation vapor pressure (kPa), and e_a is the hourly actual vapor pressure (kPa). Zotarelli et al. (2010) have presented a detailed guideline for the step-by-step calculation of ET_o. When calculating the reference evapotranspiration, instead of using R_n as proposed by Allen et al. (1998), we have adopted an approach based on the Stephan-Boltzmann law that better reflects how shadings can affect soil surface temperature and thus net radiation (An et al., 2017). The soil moisture within the root zone has been modelled with the soil water balance method propped by Allen et al. (1998). The seasonal crop yield has been computed with Equation 6, assuming that the surface temperature changes according to Equation 5 and assuming no variation of the wind speed due to the vertical PV panels rows:

$$Y_a = HIA \sum_{i=1}^{N} c_1 \times BE \times PAR_{tot,i}(1 - e^{c_2 LAI_i})\gamma_{reg,i}, \quad (6)$$

where, Y_a (t/ha) is the actual crop yield, HIA is the adjusted harvest index at maturity, c_1 is a coefficient equal to 0.001, BE is the biomass–energy ratio ((kg/ha)/(MJ/m2)), $PAR_{tot,i}$ is the total intercepted daily PAR (MJ/m^2), c_2 is a coefficient, LAI_i is the daily leaf area index (m^2/m^2), and $\gamma_{reg,i}$ is the daily crop growth-regulating factor. $\gamma_{reg,i}$ is the lowest value among the daily water, temperature, aeration, and nutrient stresses. Equation 6 is the main engine of the Environmental Policy Integrated Climate (EPIC) crop model developed by Williams et al. (1989), and it is also the central equation used in the integrated model developed by Campana et al. (2021) to simulate and optimize agrivoltaic systems. Compared to the study by Campana et al. (2021), crop yield estimation in this study was calculated with a grid resolution of 25 cm x 25 cm. Concerning crop yield, this might also be affected by the interference that the PV modules' supporting structure has on the precipitation distribution and soil moisture. This effect has not been considered or modelled in this study. Thus, vertically mounted agrivoltaic systems do not affect the soil water balance model. The crop studied in this study is potato, one of the crops already studied by Campana et al. (2021). The critical parameters of the crop model for the selected crop can be found in the study by Campana et al. (2021). Sowing and harvesting

dates for potatoes were taken by Pulatov et al. (2015), which are the 1st of May and the 1st of October, respectively.

2.3 Data for validation

The model described in section 2.1 has been validated in two ways. A first validation has been performed using PAR data measured. Figure 4 shows the layout of the installed PAR and GHI sensors within the agrivoltaic system. In contrast, Figure 5 shows pictures of the reference PAR/PAR diffuse (PARd) and GHI/diffuse horizontal irradiance (DHI) sensors installed close to the automatic weather station (hereafter called PAR reference sensor) and the PAR sensors within the agrivoltaic system. The measurements from two PAR sensors installed at the ground level, one at 2.5 m from the vertical bifacial row (hereafter called PAR edge sensor) and one at 5 m from the vertical bifacial row (hereafter called PAR middle sensor), have been used to validate the model for high spatial resolution of PAR distribution at ground level. The installed PAR sensors are CS310 full-spectrum quantum sensors from Apogee/Campbell Scientific. The PAR/PARd is a BF5 Sunshine Sensor from Delta-T Devices. The GHI/DHI sensor is an SPN1 Sunshine Pyranometer from Delta-T Devices. The other solar radiation sensors in Figure 4 refer to Sensor Box Professional Plus from Solar-Log. All the PAR sensors are connected to a Campbell Scientific CR1000X data logger. The original PAR measurements were carried out at a 1-minute resolution for the reference and ground sensors. This study aggregates the original measurements at a 1-hour time resolution for computational time constraints. Further cross-validation has been performed using the commercial software DL-Light®, an extension of SketchUp® that uses a ray-tracing approach to calculate surface radiation. Since the agrivoltaic system in Kärrbo Prästgård entered operation in May 2021 and its related monitoring system in June 2021, the PAR validation presented under Section 3 refers to only a few representative days. To calculate the PAR distribution at high resolution at the crop level during the growing season, we have used PAR data from the Strång model (Strång, 2022). The cross-validation with DL-Light® has been performed using GHI data for a typical meteorological year is taken from the Meteonorm database (Meteonorm, 2022) instead of PAR or GHI-measured data. This comparison has also been performed because challenges have been encountered while modifying the original DL-Light® input file that uses GHI data with PAR data. Presumably, this was due to internal routines of DL-Light® for checking data quality. DL-Light® is commonly used to simulate natural and interior lighting conditions in the architectural context. Direct and diffuse irradiance components are tracked, including reflections based on specified material properties.

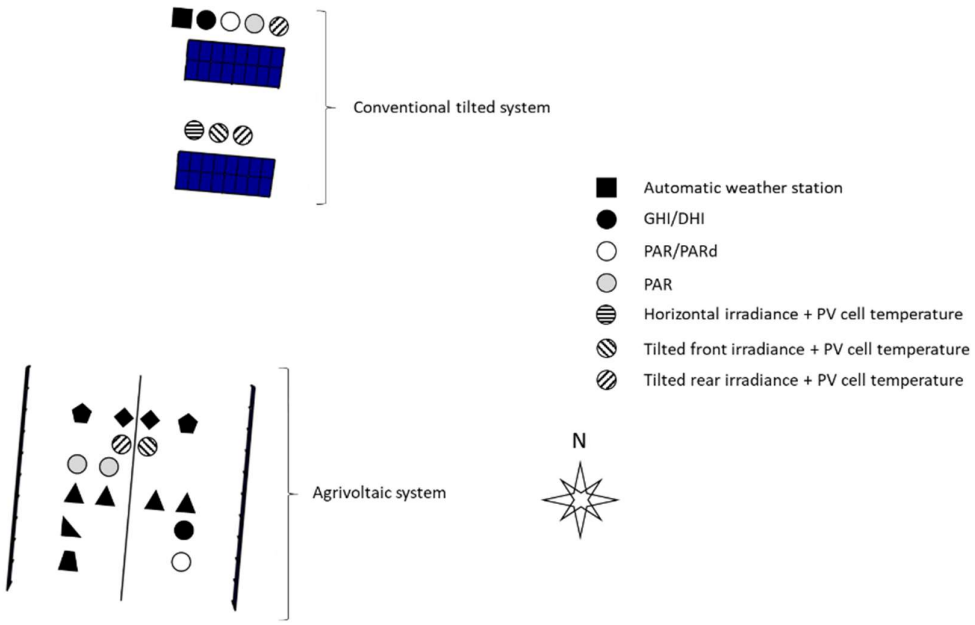

Figure 4: The solar irradiance monitoring layout at the end of 2022 at the experimental agrivoltaic facility.

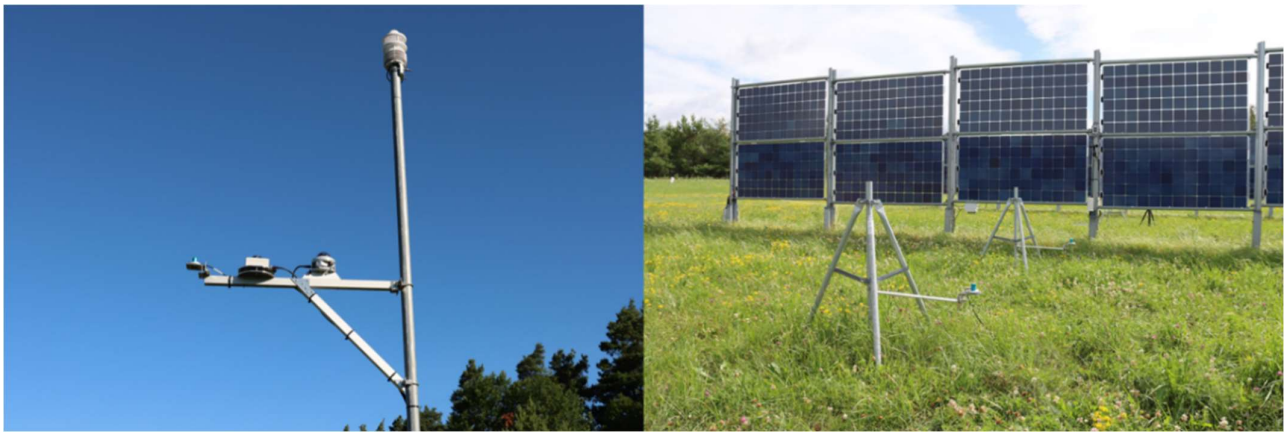

Figure 5: Photo of the PAR, PAR/PAR_d, and GHI/DHI sensors (from left to right) installed on the same mast of the automatic weather station (left) and PAR sensors at the ground level.

3 Results and discussion

In this section, the validation and cross-validation, respectively, for PAR and GHI distributions at ground level are presented. Afterwards, the application of the model for surface temperature, reference evapotranspiration, and crop yield distributions are presented.

3.1 Photosynthetically active radiation distribution model validation

The PAR seasonal distribution (i.e., from April to September included) from where the modelled hourly time series of PAR are extracted for validating the calculated PAR time series at the PAR middle and edge sensors is shown in Figure 6. Figure 6 has been produced using the available PAR measured data from the PAR reference sensor and PAR data retrieved from Strång (2022). A complete time series was not available since the PAR reference and PAR middle and edge sensors were installed in June 2021. Moreover, PAR middle and edge sensors are sometimes removed during the crop growing season for performing agricultural activities. The PAR middle and edge sensors are also removed outside of the crop growing season to avoid the harsh ground winter conditions and possibility of thefts. The validation of the PAR distribution model is presented in Figure 7 for three consecutive clear sky days for the PAR middle sensor, one overcast day, and three consecutive clear sky days for the PAR edge sensor, respectively. A further comparison between measured and modelled data for the PAR sensors installed close to the ground is depicted in Figure 8 as scatter plots. The measured data contained in Figure 8

refers to the measurements available during the crop growing seasons in 2021 and 2022. The error metrics, including the coefficient of determination (R^2), the root mean square error (RMSE), the mean absolute error (MAE), and mean bias error (MBE), are superimposed in Figure 8. Figures 7 and 8 show that the model developed in this study tends to underestimate the PAR at the sensors' locations compared to the ground measurements. There are three potential reasons for the underestimation:

1. Lack of accurate computation of the reflected irradiance that can have a significant impact, especially in vertically mounted agrivoltaic systems
2. Field conditions, especially for the PAR sensors mounted close to the ground that are typically exposed to dust connected to agricultural and experimental activities. Further minor interferences at sunrise and sunset could also be caused by the supporting structure used for the PAR middle and edge sensors (see Figure 5).

One field activity that is difficult to track and model and might have a significant effect on the solar radiation distribution and the accuracy of the simulations is the presence of grass underneath the vertical supporting structure. This grass is sometimes left by the farmer carrying out agricultural activities, but sometimes it is removed. The effects of those maintenance practices are presented in more detail in Section 3.2 while plotting and validating the GHI distributions with or without grass underneath the supporting structure. Concerning the

sensors' measurements connected to field conditions, it can be noted from Figure 7 that there is a discrepancy during noon between the measured values of the PAR reference sensor and the measured values at the PAR sensors installed close to the ground. On the other hand, it can be noted that a good agreement is shown between the peak modelled PAR and the peak measured PAR at the PAR reference sensor. The discrepancy between peak measured PAR at the reference sensor as compared to the ground level and the good agreement between peak measured PAR at the reference sensor and peak modelled PAR further strengthens that the model PAR underestimation is mostly connected to the field conditions to which the ground-mounted PAR sensors are subjected. Significantly better accuracies could be achieved with daily sensor cleaning operations. Another aspect worthy of note is that there is an evident difficulty from the model to capture the exact moment where shading appears-disappears, especially in the PAR edge sensor (e.g., discrepancy occurring between modelled PAR and measured PAR at low PAR measured values [e.g., left part of the second subplot]). This discrepancy can be caused by the difficulty in tracking operational field activities connected to the grass removal underneath the supporting structure. The presence or not of grass underneath the supporting structure can affect the reflected radiation on the PAR sensors installed close to the ground. Moreover, the geometrical model developed in this study in Matlab® environment is a simplification of reality. In reality, gaps between the vertically mounted bifacial PV modules allow light to go through the PV array and reach the PAR sensors. Furthermore, the bifacial PV modules do not form a perfect plane, but each two PV modules in the vertical direction are staggered by some centimetres compared to the following and preceding PV modules (see Figure 5). These geometrical details are not represented in the geometrical model of the agrivoltaic system implemented in the code developed in this study but could affect the modelled shading distribution compared to reality. Those details, as mentioned above, and their effects on the shading distribution can be captured on sub-hourly simulations. Nevertheless, we have performed hourly simulations in this study, and the original 1-minute measurements have been aggregated hourly. This time issue could introduce other errors in comparing modelled and measured data.

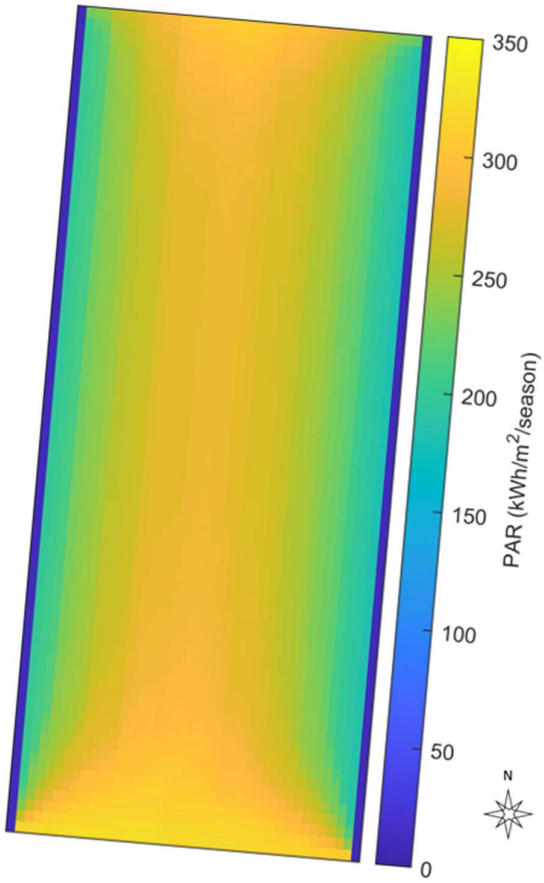

Figure 6: PAR seasonal distribution within the agrivoltaic system at Kärrbo Prästgård in 2021.

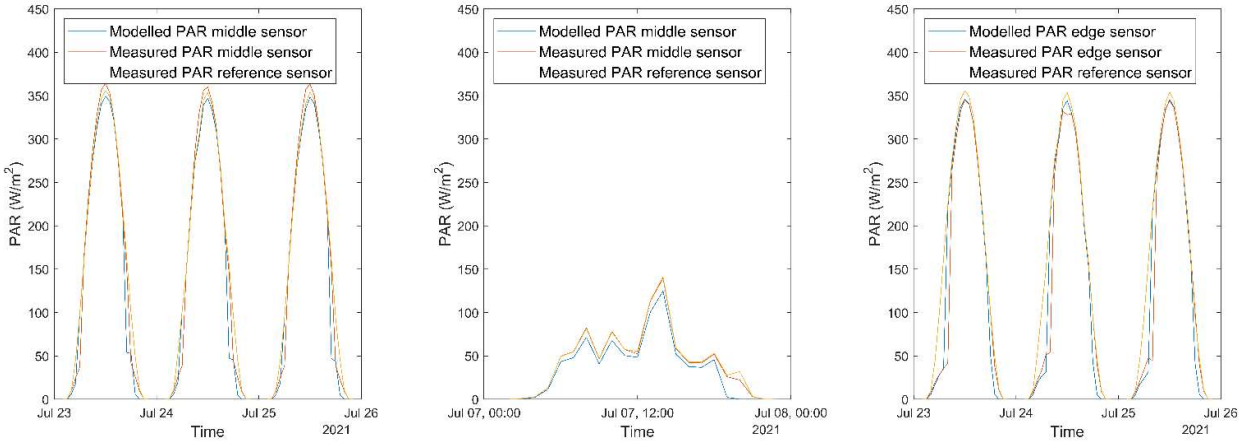

Figure 7: Validation of the PAR distribution model for the PAR middle sensor for three consecutive clear-sky days at the PAR middle sensor (left), for one overcast day at the PAR middle sensor(middle), and for three consecutive clear-sky days at the PAR edge sensor (right).

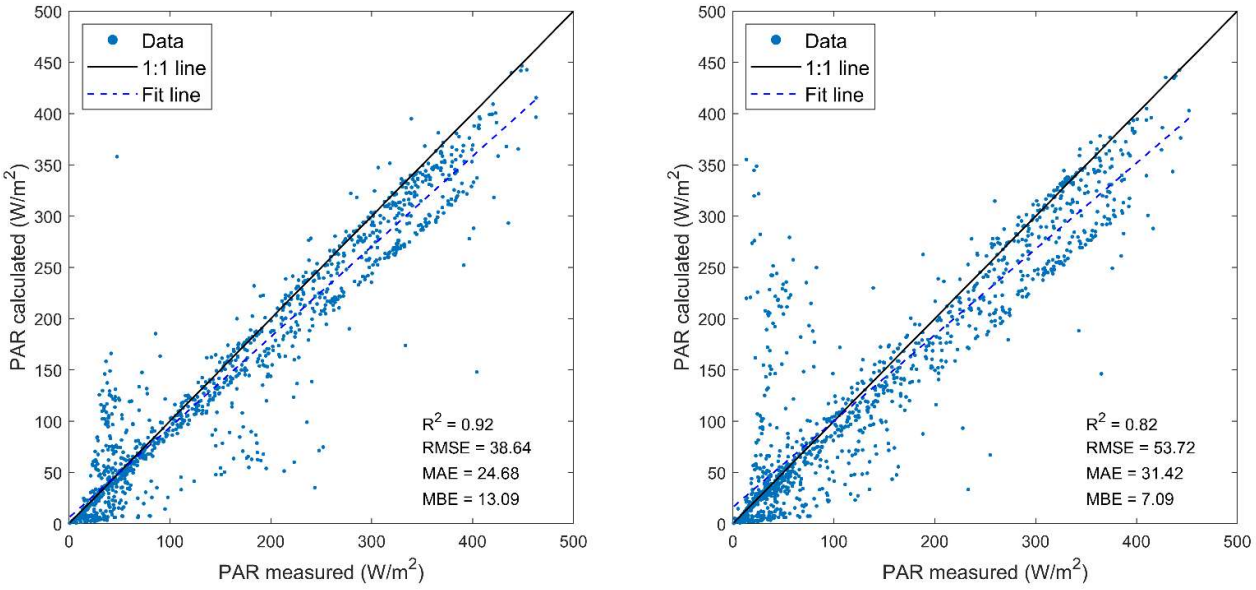

Figure 8: Scatter plot of the measured versus calculated PAR at the middle (left) and edge (right) sensors.

3.2 Global horizontal irradiance distribution model cross-validation

Two scenarios were considered when analysing the GHI distribution at ground level: with and without grass underneath the supporting structure. The aspect of how the presence or absence of grass underneath the supporting structure affects the solar irradiance distribution was already highlighted and partially shown in the study by Campana et al. (2021). The 3D models developed in SketchUp® and used as a basis for ray-tracing calculations with the DL-Light® Watt extension, are depicted in Figure 9. The simulations were performed using the same temporal range and geometry as in the proposed Agri-OptiCE model with a grid resolution of 25 cm x 25 cm. The ground albedo was assumed to be the default 0.2 for grass. Interreflections were not considered. The data depicted in Figure 9 and following have been calculated using typical meteorological year data taken from the Meteonorm database (Meteonorm, 2022). The model used for cross-validation represents a row of a vertically mounted agrivoltaic system with PV modules East-West oriented (i.e., it does not completely reflect the orientation of the experimental agrivoltaic facility [see Figures 4 and 6]). It can be clearly seen that the radiation distribution at ground level can be significantly affected by the presence of grass or not. For cross-validation, two ground-based points were selected. Those two points correspond to the exact location of the PAR middle and edge sensors within the agrivoltaic system, but the height is at ground level. The comparison between modelled data with DL-Light® taken as reference

and modelled data with Agri-OptiCE is presented in Figures 10-11 for the case with and without grass, respectively. The error metrics, including R^2, RMSE, MAE, and MBE, are superimposed.

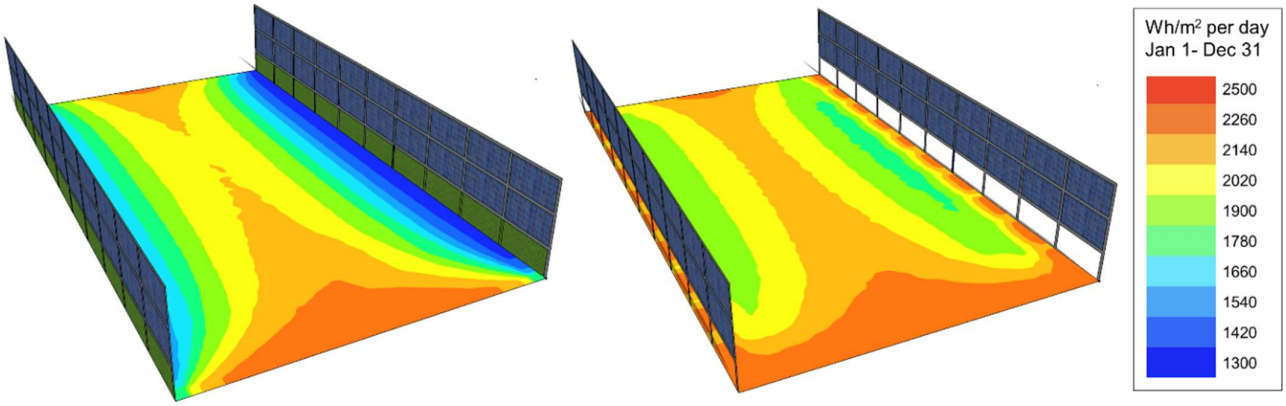

Figure 9: 3D models developed in SketchUp® and for the vertically mounted agrivoltaic system with and without grass underneath of the PV modules supporting structure.

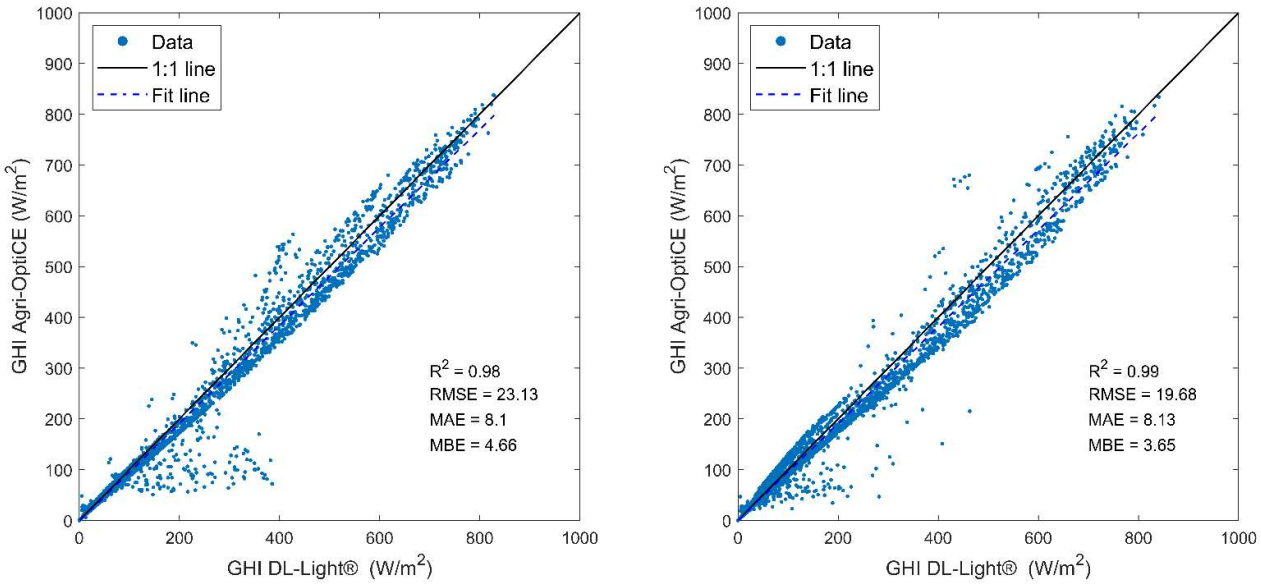

Figure 10: Comparison between DL-Light® and Agri-OptiCE Global horizontal irradiance (GHI) distribution for the middle (left) and edge (right) sensors assuming grass underneath the agrivoltaic system supporting structure.

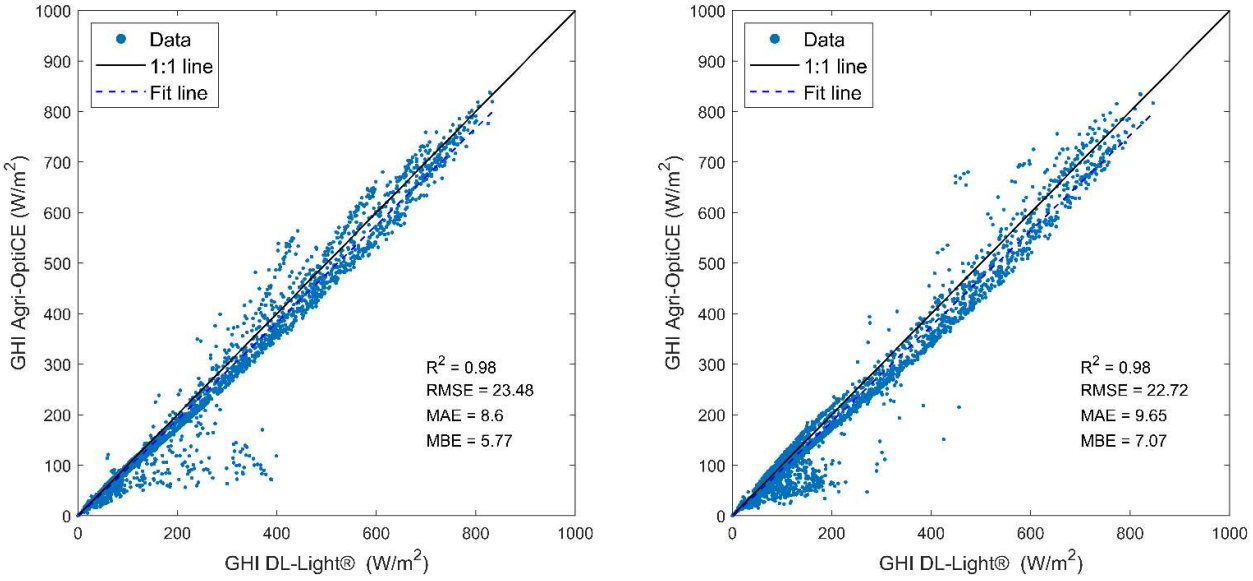

Figure 11: Comparison between DL-Light® and Agri-OptiCE Global horizontal irradiance (GHI) distribution for the middle (left) and edge (right) sensors assuming no grass underneath the agrivoltaic system supporting structure.

Figures 10-11 clearly show that the model developed in this study shows high accuracy (i.e., R^2 higher than 0.98) in all the cases and sensor positions considered. As it occurred for the PAR measurements validation, a loss in accuracy occurs while the sensors pass from shading to a non-shading condition and vice versa.

3.3 Model applications

The distribution of the surface temperature and reference evapotranspiration for a specific day and hour are depicted in Figure 12a. Figures 12a and the following ones have been computed assuming the grass is left underneath the agrivoltaic structure. As performed for the cross validation, the data depicted in Figure 12 have been calculated using typical meteorological year data taken from the Meteonorm database (Meteonorm, 2022). The geometrical of the agrivoltaic system represents a row of a vertically mounted agrivoltaic system with PV modules East-West oriented (i.e., it does not completely reflect the orientation of the experimental agrivoltaic facility [see Figures 4 and 6]). The surface temperature is a fundamental parameter for calculating the crop temperature stress and assessing the microclimate underneath agrivoltaic systems that can affect the energy performances of the bifacial PV modules. This study estimated the surface temperature with Equation 4 from Remund et al. (2018). They reported an R^2 of 0.87 against measurements. A more detailed model for estimating surface

temperature was developed by Leaf and Erell (2018) by using an energy balance approach, and they reported an R^2 of 0.95. A natural evolution of the code developed in this study will be to implement the model by Leaf and Erell (2018) for estimating surface temperature. Reference evapotranspiration represents another fundamental parameter/step for calculating crop water requirements and, consequently, soil moisture and crop water stresses under agrivoltaic systems. As it was presented for PAR and GHI distribution, the presence of the agrivoltaic system affects the distribution of the average surface temperature and cumulative reference evapotranspiration between the two adjacent rows of bifacial PV modules. The variation of annual mean surface temperature and cumulative reference evapotranspiration as compared to the reference non-shaded area is depicted in Figure 12b. The parts of the agrivoltaic rows that suffer the most reduction in solar irradiance are the same parts for which the mean surface temperature and annual evapotranspiration have lowest values. The crop yield distribution for potatoes can be found in Figure 12c, together with the average soil moisture depletion (i.e., root zone depletion Dr,i as formulated in Allen et al. [1998]). A similar trend is also shown here, with the crop yield higher in the middle of the row where the crops receive higher values of PAR than the edges.

The model developed by Campana et al. (2021) calculated the average crop yield under the agrivoltaic as a function of the row distance, average shading factors, and corresponding reductions in PAR, and reference evapotranspiration. The computed average crop yield under the agrivoltaic along the central area is 5.74 t/ha with the model developed in this study. The crop yield calculated with the model developed by Campana et al. (2021) is 5.9 t/ha. It can be concluded that the model developed by Campana et al. (2021), despite using a simplified approach within the entire area delimited by two rows, shows a satisfactory accuracy compared to the more advanced model presented in this study. Due to the lack of statistics concerning potato yield in open-field conditions in Västmanland County (the county where the experimental agrivoltaic facility is installed), the average potato yield in the Orebro County, one of the closest counties to Västmanland County, was taken as reference. The average potato yield in the period 2011-2021 is 30.7 t/ha (Statistic Sweden, 2022). By assuming a 20% dry matter weight, this totals 6.140 t/ha. The maximum and minimum reported crop yield in open-field conditions were 7.348 t/ha and 5.044 t/ha (Statistic Sweden, 2022). A more detailed validation for a specific year was carried out in the study by Campana et al. (2021).

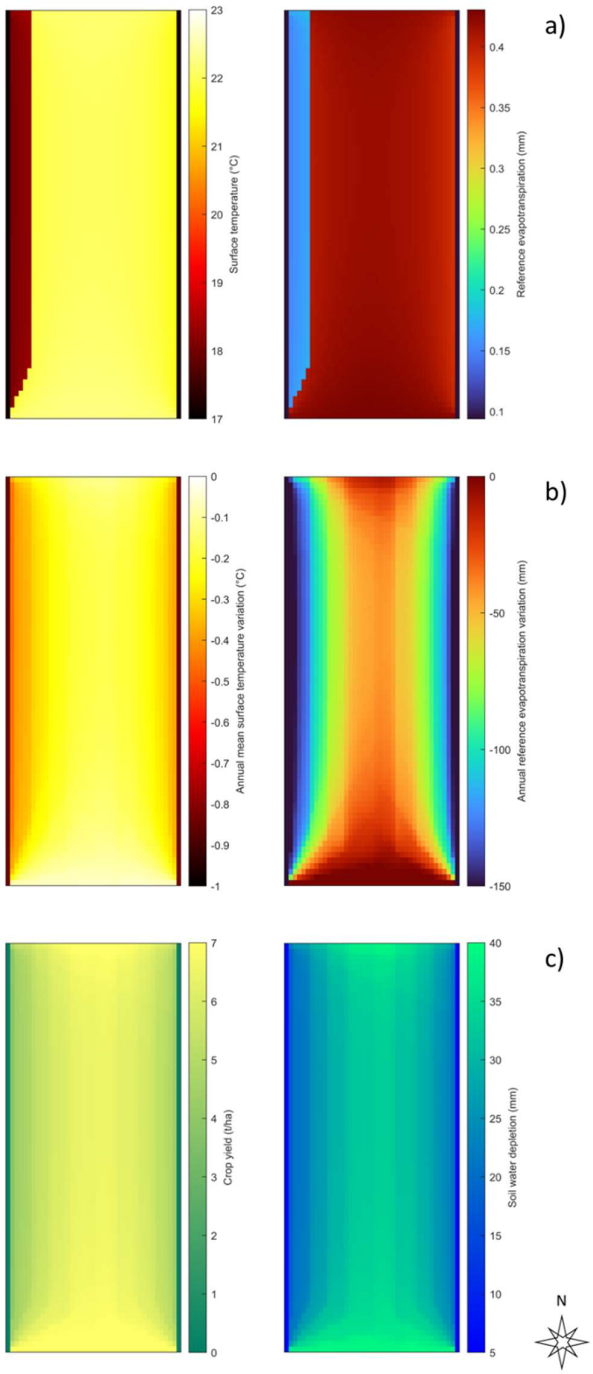

Figure 12: a) Surface temperature (left) and reference evapotranspiration (right) distribution for one single hour (i.e., June 15th 11 am) for a typical meteorological year; b) Annual mean surface temperature variation compared to the reference non-shaded area (left) and cumulative reference evapotranspiration variation compared to the reference non-shaded area (right) for a typical meteorological year; c) Crop yield distribution and average soil moisture depletion within the agrivoltaic field for potato.

As mentioned in Section 2.2, the effect of wind on the precipitation and soil moisture distributions in this study has not been considered. This effect could potentially have significant effects, especially in vertically mounted agrivoltaic systems, since they might represent a barrier to the precipitation, mainly when precipitation occurs in combination with high wind speeds. Thus, we normalized wind speed intensity and precipitation and calculated the product during the crop growing season. Figure 13 shows the normalized product rose.

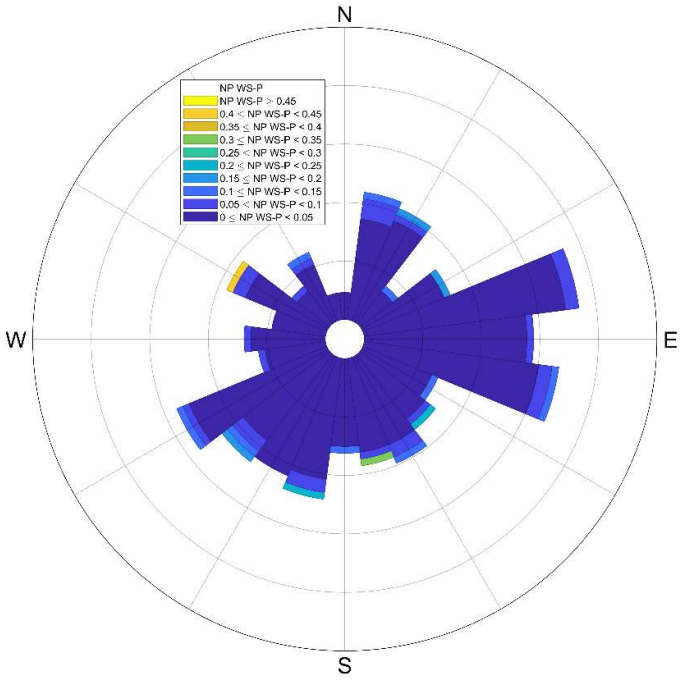

Figure 13: Normalized product wind speed-precipitation rose during the crop growing season (i.e., from April to September).

It can be clearly seen that the occurrence of the highest wind speeds and precipitations has a marked direction, mainly from the East. This wind-precipitation distribution shows that the soil in correspondence of the East side of the PV modules row can have a rain accumulation effect and thus higher soil moisture values than the West side. This heterogeneous distribution of the precipitation can affect water stresses and crop yield depending on the season. For instance, during a dry season, the soil on the East side of the PV modules row can benefit from water accumulation, while the West side can further suffer a lack of water. On the other hand, during a wet season, the soil on the East side of the PV modules row can suffer from aeration stress, while the West side can benefit from the lack of water.

4 Conclusions and future works

This study developed a model for high-resolution spatial distribution of PAR and GHI at the crop level from an existing model for simulation and optimization of vertically mounted agrivoltaic systems. The main conclusion of this study are as follows:

- The modelled high spatial resolution PAR is higher than the measured PAR at ground level, with coefficients of determination varying from 0.82 to 0.92 for PAR edge and PAR middle sensors, as defined in the main text. By analysing the mismatch between measured PAR values at the reference sensor and measured PAR values at the ground level during noon, it can be concluded that field conditions could be a primary cause of the mismatch between measured and modelled PAR at ground level.
- The modelled high spatially resolution GHI shows good agreement with the commercial software DL-Light®, an extension of SketchUp® that uses a ray-tracing approach to calculate radiation on surfaces with coefficients of determination higher than 0.98
- Among several model applications presented in this study, the computation of crop yield between two adjacent rows of the vertically mounted agrivoltaic system shows good agreement with an existing integrated model for the simulation and optimization of agrivoltaic systems.
- The computation of the soil moisture within the agrivoltaic system can be significantly affected by the combined effects of wind speed, direction, and precipitation, and thus this aspect should be carefully investigated.

Acknowledgments

The first author acknowledges Formas - a Swedish Research Council for Sustainable Development, for the funding received through the early career project "Avoiding conflicts between the sustainable development goals through agro-photovoltaic systems", grant number FR-2021/0005. The authors also acknowledge the financial support received from the Swedish Energy Agency through the project "Evaluation of the first agrivoltaic system in Sweden", grant number 51000-1. This project allowed the main establishment of the agrivoltaic experimental facility used in this study. The authors also acknowledge the funding received from the Swedish Energy Agency through the project "SOLVE", grant number 52693-1. Furthermore, the authors acknowledge the Future Energy Center at Mälardalen University for the internal projects "World-class agrivoltaic system" and "Enhancing the scientific relevance and safety of the first

agrivoltaic system in Sweden" to have significantly improved the solar radiation monitoring within the agrivoltaic system experimental facility at Kärrbo Prästgård.

References

Al Mamun, Mohammad Abdullah, et al. "A review of research on agrivoltaic systems." Renewable and Sustainable Energy Reviews 161 (2022): 112351.

Allen, R. G., Pereira, L. S., Raes, D., & Smith, M. (1998). Crop evapotranspiration-Guidelines for computing crop water requirements-FAO Irrigation and drainage paper 56. Fao, Rome, 300(9), D05109.

Amaducci, S., Yin, X., & Colauzzi, M. (2018). Agrivoltaic systems to optimise land use for electric energy production. Applied energy, 220, 545-561.

An, N., Hemmati, S., & Cui, Y. J. (2017). Assessment of the methods for determining net radiation at different time-scales of meteorological variables. Journal of Rock Mechanics and Geotechnical Engineering, 9(2), 239-246.

Barron-Gafford, G. A., Pavao-Zuckerman, M. A., Minor, R. L., Sutter, L. F., Barnett-Moreno, I., Blackett, D. T., ... & Macknick, J. E. (2019). Agrivoltaics provide mutual benefits across the food–energy–water nexus in drylands. Nature Sustainability, 2(9), 848-855.

Campana, P. E., & Lawford, R. (2022). Renewable energies in the context of the water-food-energy nexus. In Complementarity of Variable Renewable Energy Sources (pp. 571-614). Academic Press.

Campana, P. E., Stridh, B., Amaducci, S., & Colauzzi, M. (2021). Optimisation of vertically mounted agrivoltaic systems. Journal of Cleaner Production 325 (2021) 129091

Cascone, Y., Corrado, V., & Serra, V. (2011). Calculation procedure of the shading factor under complex boundary conditions. Solar Energy, 85(10), 2524-2539.

Cheng, S. J., Bohrer, G., Steiner, A. L., Hollinger, D. Y., Suyker, A., Phillips, R. P., & Nadelhoffer, K. J. (2015). Variations in the influence of diffuse light on gross primary productivity in temperate ecosystems. Agricultural and Forest Meteorology, 201, 98-110.

Deline, C., MacAlpine, S., Marion, B., Toor, F., Asgharzadeh, A., & Stein, J. S. (2016, June). Evaluation and field assessment of bifacial photovoltaic module power rating methodologies. In 2016 IEEE 43rd Photovoltaic Specialists Conference (PVSC) (pp. 3698-3703). IEEE.

Elamri, Y., Cheviron, B., Mange, A., Dejean, C., Liron, F., & Belaud, G. (2018). Rain concentration and sheltering effect of solar panels on cultivated plots. Hydrology and Earth System Sciences, 22(2), 1285-1298.

Gu, L., Fuentes, J. D., Shugart, H. H., Staebler, R. M., & Black, T. A. (1999). Responses of net ecosystem exchanges of carbon dioxide to changes in cloudiness: Results from two North American deciduous forests. Journal of Geophysical Research: Atmospheres, 104(D24), 31421-31434.

Hansen, C. W., Gooding, R., Guay, N., Riley, D. M., Kallickal, J., Ellibee, D., ... & Stein, J. S. (2017, June). A detailed model of rear-side irradiance for bifacial PV modules. In 2017 IEEE 44th Photovoltaic Specialist Conference (PVSC) (pp. 1543-1548). IEEE.

Hansen, C. W., Stein, J. S., Deline, C., MacAlpine, S., Marion, B., Asgharzadeh, A., & Toor, F. (2016, June). Analysis of irradiance models for bifacial PV modules. In 2016 IEEE 43rd Photovoltaic Specialists Conference (PVSC) (pp. 0138-0143). IEEE.

Horowitz, K., Ramasamy, V., Macknick, J., & Margolis, R. (2020). Capital Costs for Dual-Use Photovoltaic Installations: 2020 Benchmark for Ground-Mounted PV Systems with Pollinator-Friendly Vegetation, Grazing, and Crops (No. NREL/TP-6A20-77811). National Renewable Energy Lab.(NREL), Golden, CO (United States).

Jakubiec, J. A. (2016, July). Building a database of opaque materials for lighting simulation. In PLEA 2016–Cities, Buildings, People: Towards Regenerative Environments, Proceedings of the 32nd International Conference on Passive and Low Energy Architecture.

Jakubiec, J. A. (2022). Data-Driven Selection of Typical Opaque Material Reflectances for Lighting Simulation. LEUKOS, 1-14.

Johansson, F., Gustafsson, B. E., Stridh, B., & Campana, P. E. (2022). 3D-thermal modelling of a bifacial agrivoltaic system: a photovoltaic module perspective. Energy Nexus, 5, 100052.

Katsikogiannis, O. A., Ziar, H., & Isabella, O. (2022). Integration of bifacial photovoltaics in agrivoltaic systems: A synergistic design approach. Applied Energy, 309, 118475.

Ketzer, D., Weinberger, N., Rösch, C., & Seitz, S. B. (2020). Land use conflicts between biomass and power production–citizens' participation in the technology development of Agrophotovoltaics. Journal of Responsible Innovation, 7(2), 193-216.

Koblick. D.C. (2009). SolarAzEl.m: Solar azimuth and elevation, computer software. Available at: https://www.mathworks.com/matlabcentral/mlc-downloads/downloads/submissions/23190/versions/1/previews/SPOT/SolarAzEl.m/index.html. Accessed 4th March 2022

Kuo, C. Y., Wang, R. J., Lin, Y. P., & Lai, C. M. (2020). Urban design with the wind: pedestrian-level wind field in the street canyons downstream of parallel high-rise buildings. Energies, 13(11), 2827.

Leaf, J. S., & Erell, E. (2018). A model of the ground surface temperature for micrometeorological analysis. Theoretical and Applied Climatology, 133(3), 697-710.

Lo, C. K., Lim, Y. S., & Abd Rahman, F. (2015). New integrated simulation tool for the optimum design of bifacial solar panel with reflectors on a specific site. Renewable Energy, 81, 293-307.

Lu, S. M., Zainali, S., Stridh, B., Avelin, A., Amaducci, S., Colauzzi, M., & Campana, P. E. (2022). Photosynthetically active radiation decomposition models for agrivoltaic systems applications. Solar Energy.

Marion, B. (2020, June). Albedo data sets for bifacial PV systems. In 2020 47th IEEE Photovoltaic Specialists Conference (PVSC) (pp. 0485-0489). IEEE.

Marrou, H., Wéry, J., Dufour, L., & Dupraz, C. (2013). Productivity and radiation use efficiency of lettuces grown in the partial shade of photovoltaic panels. European Journal of Agronomy, 44, 54-66.

Martinez, I. Radiative View Factors. 2013. Available at: http://webserver.dmt.upm.es/~isidoro/tc3/Radiation%20View%20factors.pdf. Accessed 4th March 2022

Melo, E. G., Almeida, M. P., Zilles, R., & Grimoni, J. A. (2013). Using a shading matrix to estimate the shading factor and the irradiation in a three-dimensional model of a receiving surface in an urban environment. Solar energy, 92, 15-25.

Meteonorm. (2022). Available at: https://meteonorm.com/en/. Accessed 4th March 2022

Pelaez, S. A., Deline, C., MacAlpine, S. M., Marion, B., Stein, J. S., & Kostuk, R. K. (2018). Comparison of bifacial solar irradiance model predictions with field validation. IEEE Journal of Photovoltaics, 9(1), 82-88.

Perez, R., Ineichen, P., Seals, R., Michalsky, J., Stewart, R., 1990. Modeling daylight availability and irradiance components from direct and global irradiance. Sol. Energy, 44(5), 271-289.

Perez, R., Seals, R., Ineichen, P., Stewart, R., Menicucci, D., 1987. A new simplified version of the Perez diffuse irradiance model for tilted surfaces. Sol. Energy, 39(3), 221-231.

Pulatov, B., Linderson, M. L., Hall, K., & Jönsson, A. M. (2015). Modeling climate change impact on potato crop phenology, and risk of frost damage and heat stress in northern Europe. Agricultural and Forest Meteorology, 214, 281-292.

Quaschning, V., & Hanitsch, R. (1995, September). Shade calculations in photovoltaic systems. In ISES Solar World Conference (pp. 11-15).

Remund, J., Müller, S., Kunz, S., Huguenin-Landl, B., Studer, C., & Cattin, R. Meteonorm Handbook part II: Theory, Global Meteorological Database Version 7 Software and Data for Engineers, Planers and Education (2018). URL http://www. meteonorm. com.

Riedel-Lyngskær, N., Berrian, D., Alvarez Mira, D., Aguilar Protti, A., Poulsen, P. B., Libal, J., & Vedde, J. (2020). Validation of Bifacial Photovoltaic Simulation Software against Monitoring Data from Large-Scale Single-Axis Trackers and Fixed Tilt Systems in Denmark. Applied Sciences, 10(23), 8487.

Riedel-Lyngskær, N., Ribaconka, M., Pó, M., Thorseth, A., Thorsteinsson, S., Dam-Hansen, C., & Jakobsen, M. L. (2022). The effect of spectral albedo in bifacial photovoltaic performance. Solar Energy, 231, 921-935.

Sandia National Laboratories. (2022) Available at: https://pvpmc.sandia.gov/applications/pv_lib-toolbox/, Accessed 18th January 2022

Sieber, P., Böhme, S., Ericsson, N., & Hansson, P. A. (2022). Albedo on cropland: Field-scale effects of current agricultural practices in Northern Europe. Agricultural and Forest Meteorology, 321, 108978.

SolarPower Europe (2022): Global Market Outlook for Solar Power 2022-2026

Spectral Materials Database. (2022). Available at: https://spectraldb.com/. Accessed 2nd October 2022.

Spitters, C.J.T., Toussaint, H.A.J.M., Goudriaan, J., 1986. Separating the diffuse and direct component of global radiation and its implications for modeling canopy photosynthesis Part I. Components of incoming radiation. Agric. For. Meteorol. 38, 217–229.

Statistic Sweden. (2022). Available at: https://www.statistikdatabasen.scb.se/pxweb/sv/ssd/START__JO__JO0601/SkordarL2/. Accessed 20th September 2022.

Strång. (2022). Available at: https://strang.smhi.se/. Accessed 4th March 2022

Sun, X., Khan, M. R., Deline, C., & Alam, M. A. (2018). Optimization and performance of bifacial solar modules: A global perspective. Applied energy, 212, 1601-1610.

Tomei, J., & Helliwell, R. (2016). Food versus fuel? Going beyond biofuels. Land use policy, 56, 320-326.

Trommsdorff, M., Kang, J., Reise, C., Schindele, S., Bopp, G., Ehmann, A., ... & Obergfell, T. (2021). Combining food and energy production: Design of an agrivoltaic system applied in arable and vegetable farming in Germany. Renewable and Sustainable Energy Reviews, 140, 110694.

Ward, G. J. (1994, July). The RADIANCE lighting simulation and rendering system. In Proceedings of the 21st annual conference on Computer graphics and interactive techniques (pp. 459-472).

Williams, J.R., Jones, C.A., Kiniry, J.R., Spanel, D.A. The EPIC crop growth model. Transactions of the ASAE 32, (1989) 497–511

Zainali, S., Qadir, O., Parlak, S. C., Lu, S. M., Avelin, A., Stridh, B., & Campana, P. E. (2022). Computational fluid dynamics modelling of microclimate for a vertical agrivoltaic system. arXiv preprint arXiv:2209.01971.

Zotarelli, L., Dukes, M. D., Romero, C. C., Migliaccio, K. W., & Morgan, K. T. (2010). Step by step calculation of the Penman-Monteith Evapotranspiration (FAO-56 Method). Institute of Food and Agricultural Sciences. University of Florida.